Eur. Phys. J. E (2021) 44:140
https://doi.org/10.1140/epje/s10189-021-00145-3

THE EUROPEAN PHYSICAL JOURNAL E

Regular Article - Flowing Matter

Aspects of bulk properties of amorphous jammed disks under isotopic compression

Xinggang Zhang[1,a] and Dan Dai[2,b]

[1] Institute of Physics, Guizhou University, Guiyang, Guizhou 550025, China
[2] College of Computer Science and Technology, Guizhou University, Guiyang 550025, China

Received 14 September 2021 / Accepted 1 November 2021 / Published online 18 November 2021

Abstract By investigating the bidisperse disks under isotropic compression, we show the importance of non-affine deformation on the bulk properties of jammed disordered matter and how the mechanical properties are affected by the variation of microscopic quantities with the excess volume density $\Delta\rho_V$ and the friction coefficient μ. In theory, we derive a simple formula for the pressure of disk packings which sets up a bridge between the pressure and other statistical quantities like the contact number density and the average normal force. This pressure formula is used to derive the reduced pressure P^* and the reduced bulk modulus K^* for disk packings with linear interactions and under affine compression without new contacts. Combining theoretical formulae with Discrete Element Method (DEM) simulations, we investigate the average contact number $Z(\Delta\rho_V, \mu)$ and the average reduced overlap $\bar{U}(\Delta\rho_V, \mu)$ and give the analysis on how P^* and K^* are affected by the variation of Z and $\bar{U}$. For frictionless disk packings, we find that the affine assumption causes large deviation on Z and $\bar{U}$ relative to those of non-affine compression and therefore fails to predict the quantitative results of K^*. For packings with a fixed μ, due to the non-affine deformation, $\bar{U}$ varies approximately linear with the increasing $\Delta\rho_V$ and Z increases sharply near the jamming point and then approaches a saturation value. With a fixed $\Delta\rho_V$ and the increasing μ, $\bar{U}$ changes by a small amount while Z presents obvious decrease. The decrease of Z causes the decrease of the slope of function $P^*(\Delta\rho_V)$ and the value of K^* at a fixed $\Delta\rho_V$.

1 Introduction

Materials, such as granular matter, foams, emulsions, colloidal suspensions, can undergo jamming transition from a liquidlike state to a jammed state which acts like a solid and can withstand finite shear stresses before yielding. The nature of jammed disordered states is important to understand the behaviors of these materials [1]. Tremendous works have been performed on the geometrical and mechanical aspects of jammed disordered athermal materials over the last decades [2–4]. Probably the simplest model for the investigation of jamming is the packing of frictionless soft spheres that acts through purely repulsive contact forces. Such a system presents a well-defined jamming point φ_C in the limit of large size and its geometrical and mechanical properties near the jamming point exhibit power law as a function $\Delta\varphi = \varphi - \varphi_C$ where φ_C is the critical volume fraction [5,6]. While progresses have been made for packings of frictionless spheres in recent years [7–12], many researches are extended to more complicated systems such as frictional [13,14],nonspherical [15,17] particulate systems and systems with short-range attraction [16] .

A bulk property is an intensive property meaning that it is a local physical property of a system that does not depend on the amount of material in the system. Bulk properties of static jammed matter, for example the bulk modulus and shear modulus, are the key to understand the mechanical and acoustic properties of jammed matter and are often obtained by loading tests such as the compression and shear test. Theoretically, many bulk properties can be investigated by using effective medium theory(EMT) [18,19]. The EMT basically assumes that macroscopic quantities can be obtained by a simple coarse graining procedure over the individual contacts and the displacement field of particles is affine with the macroscopic deformation(the affine assumption). In EMT, by using the postulate of affine deformation, the relation between the deformation of each contact and the macroscopic strain tensor could be given theoretically. Therefore, the potential energy density of a deformed jammed matter as a function of the strain tensor can be given. Hence, we could derive the stress tensor and the elastic moduli of this jammed matter by inspection from the strain energy expansion. For the jammed disordered systems in which repulsive interactions are dominant, their microscopic structures

[a] e-mail: xgzhang@gzu.edu.cn (corresponding author)
[b] e-mail: 49881341@qq.com

are easily changed by weak loading. This can be seen from a simple fact that the average contact number Z increases dramatically with the increasing of the excess volume fraction $\Delta\varphi$ when $\Delta\varphi \to 0$ [3,6,24]. Therefore, the EMT may fail to predict the bulk properties of jammed disordered matter due to the breakdown of the affine assumption. A correct treatment for the prediction of bulk properties should include the non-affine deformation of particles [10,20–23]. However, even for the simplest model which is mentioned above, there is no simple theoretical way to estimate the motion of spheres in disordered systems under the non-affine deformation. The excess volume fraction $\Delta\varphi$ is often selected as the control parameter for jammed packings under isotropic compression. Resort to numerical simulations, the variation of many quantities such as the average contact number, the pressure and the bulk modulus with $\Delta\varphi$ have been investigated for systems near the jamming point [3,9,10]. Nevertheless, it is still not very clear on how the non-affine deformation and friction affect the bulk properties of jammed packings. To understand this, it is essential to deepen the investigation of the dependence of bulk properties on the microscopic quantities of jammed packings such as the average contact number and the average overlap.

In this work, we explore the bulk properties of jammed athermal systems under isotropic compression. For the simplicity, we perform theoretical analysis and DEM simulations on the packings of bidisperse frictionless and frictional soft disks with linear interactions. This paper considers the relations between the macroscopic mechanical quantities, such as the pressure and the bulk modulus, and other statistical quantities like the contact number density and the volume density. We derive these relations through microscopic and statistical analysis and compare the theoretical results with the DEM simulations. Similar to some of the previous studies [8,25],we perform our numerical simulations over a wide range of volume density. Since the force between each pair of disks is proportional to their overlap, dimensionless quantities such as the reduced average overlap and the reduced pressure are used to describe the soft disks. Based on our DEM simulations, we discuss the variation of the average contact number and the reduced average overlap with the excess volume density and investigate how these functions are affected by different type of compression (affine and non-affine) and by different friction coefficients. Finally, these numerical results and theoretical formulae are combined to understand how the reduced pressure and the reduced bulk modulus are affected by non-affine compression and friction.

2 Numerical simulation and contact model

Our studies focus on the athermal systems of bidisperse soft disks which are confined within a circular container. Athermal systems have been extensively investigated by using the Discrete Element Method [26]. In this paper, we take DEM as our main numerical method and limit our studies to the isotropic compression test on the bidisperse soft disks. Our simulation protocols are elaborated as follows.

(1) Bidisperse disks with total number N are randomly generated in a circular container with radius R_0. This system contains N_B big disks with radius r_B and N_S small disks with radius r_S. Three dimensionless quantities can be introduced to describe this system: the size ratio $\lambda = r_B/r_S$, the percentage of big disks $k_B = N_B/N$ and the percentage of small disks $k_S = N_S/N$. Evidently, $k_B + k_S = 1$. To avoid crystallization and obtain amorphous packings, we set $\lambda = 1.4$ and $k_B = k_S = 50\%$ because the critical jammed state of bidisperse disk packings with these parameter values can be seen as the maximally random state [27]. The initial configuration is at the unjammed loose state in which all disks are randomly located in the circular container without overlap and gravity, with low packing density.

(2) Isotropic compression tests can be implemented either by shrinking the container or inflating disks. In this paper, we adopt the method of shrinking the container. More specifically, the radius R of the container is decreased in a step by step manner while keeping the radii of all disks until R reaches an anticipated value R_e. Note that the spatial positions of all disks are fixed while R is decreased at the beginning of each step and the change amount of R for each step is very small. After the radius of the container is changed for each step, the container is fixed and a DEM dynamic process with energy dissipation is applied on all disks. In other words, the spatial positions of all disks will be continually renewed according to the dynamical equations of the system until a static configuration in mechanical equilibrium is obtained. Damping forces are involved in the DEM dynamic process for dissipating the energy of the system and the maximal unbalance force of the system approaching to zero is the criterion for obtaining a static configuration in mechanical equilibrium. In DEM simulations, the normal and tangential overlap between two discrete bodies, i.e. disk-disk or disk-container in this paper, are used to model the deformations of the two bodies in contact. We suppose that any two bodies interact with purely repulsive forces which can be written as functions of the amount of overlap. The relation between the contact force and the overlap is called contact model and the linear contact model is used to implement our DEM simulations. While the radius R is decreased, the packing density of the system increases and it undergoes a transition from an unjammed state to a jammed state. In this process, static configurations with different packing density of the system are obtained for further analysis.

(3) In order to calculate the ensemble average, different initial configurations are generated and then isotropically compressed to obtain static configurations for further data analysis. We then change some parameters and carry out the above DEM simulation process to investigate how the bulk properties of jammed pack-

Table 1 Major parameters of DEM simulations

Parameter	Value range
N	$2 \times 10^3 \sim 5 \times 10^3$
k_B	50%
λ	1.4
$K_n/N \cdot m^{-1}$	$1 \times 10^3 \sim 1 \times 10^6$
$K_s/N \cdot m^{-1}$	$0.5K_n$
μ	$0 \sim 10$

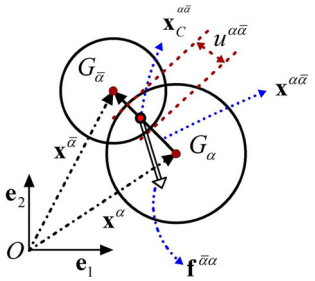

Fig. 1 The relative position and contact force between two disks. $\{\mathbf{e}_1, \mathbf{e}_2\}$ is the orthonormal basis of the Cartesian coordinate. $\mathbf{f}^{\bar{\alpha}\alpha}$ is the contact force of disk $G_{\bar{\alpha}}$ on disk G_α. $u^{\alpha\bar{\alpha}}$ is the normal overlap between $G_{\bar{\alpha}}$ and G_α

ings vary with these parameters. The major parameters of our DEM simulations are shown in Table 1.

To obtain macroscopic properties of a packing, it is important to investigate the microscopic structure and interactions between disks. Suppose that a static packing is obtained from the above DEM simulation and $\Gamma = \{(\mathbf{x}^\alpha, r^\alpha) | \alpha = 1, 2, \ldots, N\}$ is used to describe the configuration of this packing, where $\mathbf{x}^\alpha$ and r^α are the position vector and the radius of disk G_α. Let Z_α be the number of contacts of G_α and $G_{\bar{\alpha}}$ be the $\overline{\alpha}$th contact neighbor, where $\bar{\alpha} \in \{\overline{1}, \overline{2}, \ldots, \overline{Z_\alpha}\}$. As shown in Fig. 1, the position vector of disk $G_{\bar{\alpha}}$ relative to disk G_α is $\mathbf{x}^{\alpha\bar{\alpha}} = \mathbf{x}^{\bar{\alpha}} - \mathbf{x}^\alpha$ and the normal overlap between $G_{\bar{\alpha}}$ and G_α is

$$u^{\alpha\bar{\alpha}} = r^\alpha + r^{\bar{\alpha}} - x^{\alpha\bar{\alpha}} \tag{1}$$

where $x^{\alpha\bar{\alpha}} = \sqrt{\mathbf{x}^{\alpha\bar{\alpha}} \bullet \mathbf{x}^{\alpha\bar{\alpha}}}$ is the distance between the two disk centers. The position vector of the contact point between G_α and $G_{\bar{\alpha}}$ is given by

$$\mathbf{x}_C^{\alpha\bar{\alpha}} = \mathbf{x}^\alpha + (r^\alpha - \frac{u^{\alpha\bar{\alpha}}}{2})\mathbf{n}^{\alpha\bar{\alpha}} \tag{2}$$

where $\mathbf{n}^{\alpha\bar{\alpha}}$ is the unitary normal vector from G_α to $G_{\bar{\alpha}}$.

Next, we consider the interactions between disks. In our DEM simulations, linear normal and tangential contact forces with Coulomb slip condition are implemented to all contacts between disks. To obtain steady-state packings in DEM simulations, damping forces should also be involved to dissipate the kinetic energy of the system. When the configuration Γ is in mechanical equilibrium, the contact force of $G_{\bar{\alpha}}$ on G_α can be written as

$$\mathbf{f}^{\bar{\alpha}\alpha} = \mathbf{f}_n^{\bar{\alpha}\alpha} + \mathbf{f}_s^{\bar{\alpha}\alpha} \tag{3}$$

where $\mathbf{f}_n^{\bar{\alpha}\alpha}$ and $\mathbf{f}_s^{\bar{\alpha}\alpha}$ are the normal force and friction respectively. For the linear contact model, the normal contact force satisfies $\mathbf{f}_n^{\bar{\alpha}\alpha} = -K_n u^{\alpha\bar{\alpha}} \mathbf{n}^{\alpha\bar{\alpha}}$ where K_n is the normal stiffness at each contact. The shear contact force $\mathbf{f}_s^{\bar{\alpha}\alpha}$ occurs when the contact point of G_α and $G_{\bar{\alpha}}$ and the relative shear motion are formed. We write $\mathbf{f}_s^{\bar{\alpha}\alpha}$ in a compact form as

$$\mathbf{f}_s^{\bar{\alpha}\alpha} = -\min(K_s \zeta^{\alpha\bar{\alpha}}, \mu |\mathbf{f}_n^{\bar{\alpha}\alpha}|) \mathbf{t}^{\alpha\bar{\alpha}} \tag{4}$$

where K_s and μ are the shear stiffness and the friction coefficient at each contact respectively, $\zeta^{\alpha\bar{\alpha}}$ is the total tangential displacement between G_α and $G_{\bar{\alpha}}$, $\mathbf{t}^{\alpha\bar{\alpha}}$ is the unit tangential vector to the contact point. Note that we also adopt the linear contact model for contact forces between disks and the container. Through the above DEM simulations, configurations in mechanical equilibrium could be given for a disk packing under isotropic compression. Using the DEM data of a static configuration, macroscopic quantities, such as the packing density and the pressure, can be calculated.

3 Theoretical analysis

3.1 Volume density and contact number density

Considering a configuration of a particulate system in mechanical equilibrium, two distinct concepts can be defined for the description of the concentration of this packing. Volume density ρ_V is defined as the total volume of all particles divided by the volume of the container. Volume fraction φ is the total volume occupied by all particles divided by the volume of the container. In the definition of volume fraction, the total volume of intersections between particles is canceled. Evidently, ρ_V and φ have the same value when there is no deformation or intersection between any two bodies. For the bidisperse packing of disks , we have

$$\rho_V = \frac{A}{A^*} = \frac{N_B r_B^2 + N_S r_S^2}{R^2} \tag{5}$$

where A is the total area of all disks and A^* is the area of the container, R is the radius of the container, and

$$\varphi = \rho_V - \frac{A_{overlap}}{A^*} \tag{6}$$

where $A_{overlap}$ is the total area of the intersections between disks. For a packing at jamming point, ρ_{VC} and φ_C are used to indicate the critical volume density and the critical volume fraction respectively. Evidently, $0 \le \rho_V < \infty$, $0 \le \varphi \le 1$, $\varphi \le \rho_V$ and $\varphi_C = \rho_{VC}$. Note that ρ_V is more convenient than φ in most situations, since the value of ρ_V can be easily obtained

in both numerical simulations and experiments and the mathematical expressions are simpler for the relations between ρ_V and other quantities such as the mass density and the bulk modulus of a packing. Therefore, we select ρ_V as the control parameter in our DEM simulations. The average contact number is defined as

$$Z = \frac{1}{N}\sum_{\alpha=1}^{N} Z_\alpha \approx \frac{2N_C}{N} \tag{7}$$

where N_C is the total number of contacts between disks. Z is a simple but important statistical quantity for the mechanical properties of a particulate system. Defining Z is not a trivial problem since there may exist disks which do not contact with other bodies. Such kinds of disks are called rattlers and they do not contribute to the mechanical stability of the system. Apparently, all rattlers of the system are included in the formula (7) but we could also calculate Z without counting rattlers if necessary. Another important quantity is the density of contact number and it represents the number of contacts in unit volume of a particulate system. For the case of the packing of disks, the contact number density is given by

$$\rho_{NC} = \frac{N_C}{A^*} = \frac{Z\rho_V}{2\langle A_G\rangle} \tag{8}$$

where $\langle A_G\rangle = \dfrac{A}{N}$ is the average area of disks.

3.2 The definition of pressure and bulk modulus

Pressure is the most important physical quantity to describe the stress state of a jammed packing under isotropic compression. The pressure of a jammed packing can be calculated by two methods. Let f_{tot} be the total normal force of a packing on the boundary. For two dimensional systems, pressure is the force applied perpendicular to the boundary of an object per unit length. Therefore, the pressure of a jammed packing on the container is

$$P_a = \frac{f_{tot}}{2\pi R} \tag{9}$$

The second method is related to the calculation of the stress tensor according to the contact forces between disks. The average stress tensor of a packing is defined as

$$\mathbf{T} = \frac{1}{A^*}\sum_{\alpha=1}^{N}\sum_{\overline{\alpha}=\overline{1}}^{\overline{Z_\alpha}} \mathbf{f}^{\bar{\alpha}\alpha}(\mathbf{x}_C^{\alpha\overline{\alpha}} - \mathbf{x}^{\alpha}) \approx \frac{1}{A^*}\sum_{\{\alpha\overline{\alpha}\}} \mathbf{f}^{\bar{\alpha}\alpha}\mathbf{x}^{\alpha\overline{\alpha}} \tag{10}$$

Where $\sum_{\{\alpha\overline{\alpha}\}}$ is the sum over all contacts between disks and $\approx$ arises from ignoring the contacts between disks and the boundary. The pressure of a packing can be calculated by

$$P_b = \left|\frac{1}{2}tr(\mathbf{T})\right| \tag{11}$$

Note that P_a and P_b are different in their formular form, but it can be verified that P_a and P_b are statistically equivalent. Therefore, the symbol P is used to indicate P_a or P_b with ignoring the difference between them. It is more convenient to derive the macroscopic constitutive relation between the pressure and the deformation of packings by using formula (11). Calculating the trace of $\mathbf{T}$ in the formula (11) first and then considering the formulae (1) and (8) , the pressure can be written as

$$\begin{aligned} P &= \frac{1}{2A^*}\sum_{\{\alpha\overline{\alpha}\}} f_n^{\alpha\bar{\alpha}} x^{\alpha\bar{\alpha}} \\ &= \frac{1}{2}\rho_{NC}\left[\frac{1}{N_C}\sum_{\{\alpha\overline{\alpha}\}} f_n^{\alpha\bar{\alpha}}(r^{\alpha} + r^{\bar{\alpha}} - u^{\alpha\bar{\alpha}})\right] \end{aligned} \tag{12}$$

where $f_n^{\alpha\bar{\alpha}}$ is the magnitude of normal force $\mathbf{f}_n^{\bar{\alpha}\alpha}$. A new variable $D^{\alpha\bar{\alpha}} = r^{\alpha} + r^{\bar{\alpha}}$ can be defined. For convenience, we consider the normal force f_n, the sum of radii of contacting disks D and the overlap u as random variables. It is easy to see

$$P = \frac{1}{2}\rho_{NC}\langle (D-u) f_n\rangle \tag{13}$$

This formula gives the connection between the macroscopic quantity P and the statistical average of microscopic quantities and it can be easily extended to the case of three dimensional particulate packings. Since the function f_n of u is dependent on the contact model, the variation of pressure P with the deformation of packings will be affected by the contact model. Considering $\rho_V A^* = A$ and taking the derivative of it's both sides, we have

$$\mathrm{d}A^* = \frac{-A^*\mathrm{d}\rho_V}{\rho_V} \tag{14}$$

Using this formula, the bulk modulus can be given by

$$K = -A^*\frac{\mathrm{d}P}{\mathrm{d}A^*} = \rho_V\frac{\mathrm{d}P}{\mathrm{d}\rho_V} \tag{15}$$

3.3 Linear contact model and affine deformation

For the simplicity of theoretical analysis, we adopt the linear contact model to perform our DEM simulations and therefore the normal force $f_n(u) = K_n u$. For the linear contact model, it is convenient to define three dimensionless quantities: the reduced pressure $P^* = P/K_n$, the reduced overlap $U^{\alpha\bar{\alpha}} = u^{\alpha\bar{\alpha}}/D^{\alpha\bar{\alpha}}$ and

the reduced bulk modulus $K^* = K/K_n$. Using the formulae (8) and (13), one finds

$$P^* = \frac{1}{4\pi} Z\rho_V \frac{\langle D^2(U-U^2)\rangle}{\langle r^2\rangle} \tag{16}$$

For bidisperse packings, the probability distribution of r is

$$p_r(r) = k_B\delta(r-r_B) + k_S\delta(r-r_S) \tag{17}$$

Since the initial configuration of disks is generated randomly, we suppose that the joint probability distribution of the two radii r_1 and r_2 of contacting disks is

$$p_{rr}(r_1, r_2) = p_r(r_1)p_r(r_2) \tag{18}$$

Another hypothesis is that D and U are independent random variables and the probability distribution of D is irrelevant with the volume density ρ_V. Let $p_R(D)$ and $p_U(U;\rho_V)$ indicate the probability distribution of D and U respectively. We have

$$\begin{aligned} p_R(D) &= \iint \delta(D-r_1-r_2)p_{rr}(r_1,r_2)dr_1dr_2 \\ &= k_B^2\delta(D-2r_B) + 2k_Bk_S\delta(D-r_B-r_S) \\ &\quad + k_S^2\delta(D-2r_S) \end{aligned} \tag{19}$$

This formula can be verified by DEM simulations of bidisperse disks within acceptable deviation between theory and numerical results [27]. Therefore, we have

$$\frac{\langle D^2\rangle}{\langle r^2\rangle} = \frac{4\lambda^2k_B^2 + 2(\lambda+1)^2k_Bk_S + 4k_S^2}{\lambda^2k_B + k_S} \tag{20}$$

The independence of D and U causes $\langle D^2(U-U^2)\rangle = \langle D^2\rangle\langle U-U^2\rangle$. We will verify this hypothesis by numerical simulation results of bidisperse disks in the next section of this paper. Based on the above results, we have

$$P^* = \frac{1}{4\pi}\frac{\langle D^2\rangle}{\langle r^2\rangle} Z\rho_V \langle U-U^2\rangle \tag{21}$$

We will see from the results of DEM simulations that $\langle U^2\rangle \approx \langle U\rangle^2$ and $\langle U\rangle \gg \langle U^2\rangle$ over the wide range of $\triangle\rho_V$ where $\triangle\rho_V = \rho_V - \rho_{VC}$. To obtain P^* as a function of ρ_V, the functions such as $Z(\rho_V)$ and $\bar{U}(\rho_V) = \int Up_U(U;\rho_V)dU$ should be given. However, these are not trivial tasks from the theoretical aspect even for packings of disks under isotropic compression. In this paper, we use the DEM simulations to obtain these functions. If $P^*(\rho_V)$ is obtained, the reduced bulk modulus can be calculated by using the formula $K^* = \rho_V \frac{\mathrm{d}P^*}{\mathrm{d}\rho_V}$.

In our DEM simulations, the isotropic compression is implemented by changing the radius of the container R in a step by step manner while keeping the positions and radii of all disks unchanged. For each step of changing R , the renewed radius of the container is set to λR where λ is called stretch ratio. This is followed by a relaxation period to achieve a static configuration in mechanical equilibrium. The stretch ratio λ can be calculated by the volume density ρ_V and its increment $d\rho_V$. According to $\rho_V = A/(\pi R^2)$, the stretch ratio is derived as

$$\lambda = \sqrt{1 - \frac{\rho_V}{\rho_V + \mathrm{d}\rho_V}} \approx 1 - \frac{\mathrm{d}\rho_V}{2\rho_V} \tag{22}$$

For disordered packings, the process of relaxation will cause the non-affine deformation. To understand how the bulk properties are affected by non-affine deformation, it is meaningful to compare the results of non-affine compression with the one of affine compression. Therefore, we consider a virtual process which is called affine isotropic compression. An affine isotropic compression on a configuration Γ is implemented by changing the radius of the container and the position vectors of all disks according the linear transformation $\mathbf{T}_A = \begin{pmatrix} \lambda & 0 \\ 0 & \lambda \end{pmatrix}$ while keeping the radii of all disks unchanged. That is to say, if the center of the container is the origin of coordinates, the position vector of the center of each disk $\mathbf{x}$ is renewed to $\mathbf{T}_A\mathbf{x} = \lambda\mathbf{x}$ for each step of the radius shrinking of the container to λR. Note that there is no the process of relaxation following each step of the shrinking of the configuration Γ. Let $\Gamma(\rho_{VC})$ and $\Gamma_A(\rho_V)$ be the configuration at jamming point and the jammed state with volume density ρ_V respectively. We consider a series of affine isotropic compression which change the packing of disks from $\Gamma(\rho_{VC})$ to $\Gamma_A(\rho_V)$. In EMT, by using the postulate of affine deformation, it is possible to obtain the relation between the deformation of each contact and the strain tensor. Therefore, the potential energy density as a function of the strain tensor can be given. Furthermore, the stress tensor and the elastic moduli could be obtained by inspection from the strain energy expansion [18–20]. Here, to calculate the pressure and the bulk modulus of packings under the affine isotropic compression, we use a more direct method which is based on the reduced pressure formula (21). Let $Z_A(\rho_V)$ and $\bar{U}_A(\rho_V)$ be the average contact number and the average reduced overlap of $\Gamma_A(\rho_V)$ respectively. These two functions can be easily obtained by the numerical simulations of affine isotropic compression from $\Gamma(\rho_{VC})$ to $\Gamma_A(\rho_V)$, but it is difficult to derive $Z_A(\rho_V)$ and $\bar{U}_A(\rho_V)$ using pure theoretical methods. However, if we consider an imaginary affine compression in which the average contact number remain unchanged, i.e. $Z_A(\rho_V) = Z_A(\rho_{VC}) = Z_C$, the reduced pressure P^*_{AZ} and the reduced bulk modulus K^*_{AZ} for this imaginary compression can be easily derived. For convenience, we call such compression as affine compression without new contacts in this paper.

For each overlap, considering formula (1), we have

$$u + \mathrm{d}u = D - \lambda x \tag{23}$$

Substituting (22) into (23), one finds

$$\frac{\mathrm{d}u}{D-u} = \frac{\mathrm{d}\rho_V}{2\rho_V} \tag{24}$$

After integrating this formula on both sides, we have

$$u = D - (D - u_0)\sqrt{\frac{\rho_{V0}}{\rho_V}} \tag{25}$$

where u_0 is the initial overlap and ρ_{V0} is the initial volume density. Since $\Gamma(\rho_{VC})$ is the configuration at jamming point and no new contacts are generated , we have,

$$u = (1 - \sqrt{\frac{\rho_{VC}}{\rho_V}})D \tag{26}$$

This result tells us that the average overlap of a packing under the affine compression without new contacts can be related to its volume density in a very simple way. Using formula (21) and the above equation, the reduced pressure is

$$P^*_{AZ} = \frac{1}{4\pi} Z_C \frac{\langle D^2 \rangle}{\langle r^2 \rangle} \sqrt{\rho_{VC}}(\sqrt{\rho_V} - \sqrt{\rho_{VC}}) \tag{27}$$

and the reduced bulk modulus is

$$K^*_{AZ} = \frac{1}{8\pi} Z_C \frac{\langle D^2 \rangle}{\langle r^2 \rangle} \sqrt{\rho_{VC}\rho_V} \tag{28}$$

Note that new contacts could be generated even in the situation of affine compression, especially in the disordered packings. Therefore, these two formulae are tenable only for the disk packings under the affine compression without new contacts. The effects of the generating of new contacts on the bulk properties of soft disks could be given by performing numerical simulations on disk packings under affine deformation.

4 Results and discussion

4.1 Bulk properties of frictionless disks

Numerical simulations on packings of spheres are usually used to investigate the behaviors of jammed matter [2–4]. Many previous studies studied jammed solids only around jamming transition density [3,6,14]. Some of previous studies focused on a very wide range of densities and given new insights into the properties of jammed solids [8,25]. In this paper, we also perform

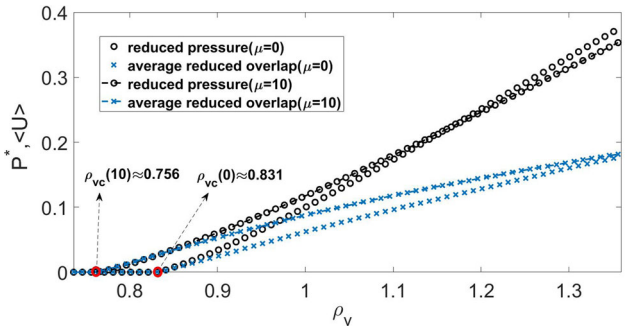

Fig. 2 Reduced pressure P^* and average reduced overlap $< U >$ vary with volume density ρ_V for the case of $\mu = 0$ and $\mu = 10$. $\rho_{VC}(\mu)$ represents the critical point of jamming transition and therefore is called critical volume density

numerical simulations over a wide range of volume density ρ_V. Note that the average contact number Z is kept not exceeding 6 in our simulations. In this part, we focus on the bulk properties of frictionless (i.e. $\mu = 0$) bidisperse disks under isotropic compression, especially the comparison between non-affine compression and affine compression. The value range of major parameters are indicated in Table 1. Note that all the results are irrelevant with the normal stiffness K_n and the total number of disks is in the large N limit.

In Fig. 2, the reduced pressure P^* is calculated by using the pressure formula P_a. The DEM results show that the packings of disks undergo a jamming transition with increasing volume density for both frictionless and frictional systems. The critical volume density can be obtained by inspection either from the curve of P^* or the curve of $< U >$. Similar to the former researches [3,14,24], the critical volume density $\rho_{VC}(\mu)$ decreases with increasing frictional coefficient μ. $\rho_{VC}(0) \approx 0.831$ is close to well-known values of random close packing of disks and $\rho_{VC}(10) \approx 0.756$ is close to values of random loose packing. Evidently, it is better to select the excess volume density $\Delta\rho_V = \rho_V - \rho_{VC} \geq 0$ as the control parameter in many discussions. If we consider functions $P^*(\Delta\rho_V)$ and $\bar{U}(\Delta\rho_V)$ where $\bar{U} =< U >$, one finds that $\bar{U}(\Delta\rho_V)$ is an approximate linear function for both frictionless and frictional systems while $P^*(\Delta\rho_V)$ is nonlinear especially at the states near the jamming point ρ_{VC}. The formula (21) was derived based on the hypothesis of the independence between the radii sum D and the reduced overlap U. To verify the independence of D and U, the correlation coefficient $Cor(D,U) = \frac{\sum_{\{\alpha\bar{\alpha}\}}(D^{\alpha\bar{\alpha}} - <D>)(U^{\alpha\bar{\alpha}} - <U>)}{\sqrt{\sum_{\{\alpha\bar{\alpha}\}}(D^{\alpha\bar{\alpha}} - <D>)^2}\sqrt{\sum_{\{\alpha\bar{\alpha}\}}(U^{\alpha\bar{\alpha}} - <U>)^2}}$ is calculated by using the DEM data for each jammed packing with different volume density. As shown in Fig. 3, $Cor(D,U)$ is very close to zero with the whole variation range of $\Delta\rho_V$. This indicates that the hypothesis of the independence of D and U is reasonable.

Using the formula (21), $P^*(\Delta\rho_V)$ can be calculated theoretically when $Z(\Delta\rho_V)$, $\bar{U}(\Delta\rho_V)$ and $\bar{U}^2(\Delta\rho_V)$ are obtained. It is not a simple task to derive these three functions by pure theoretical analysis. However,

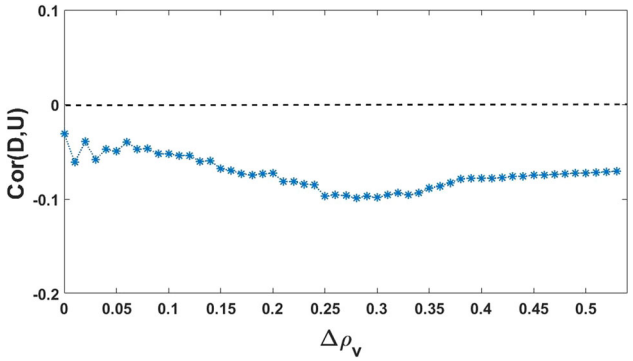

Fig. 3 Correlation coefficient between the radii sum D and the reduced overlap U varies with excess volume density $\Delta\rho_V$ for the case of $\mu = 0$

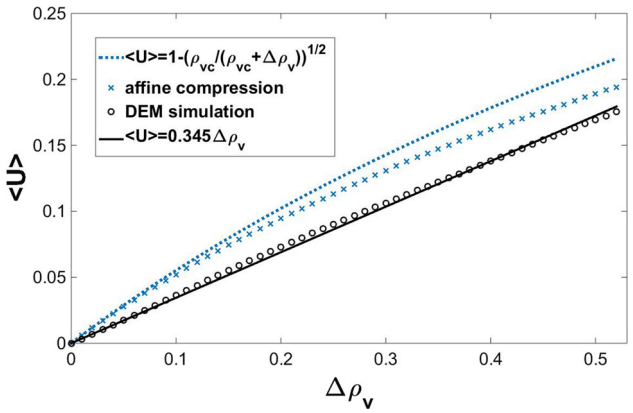

Fig. 4 Average reduced overlap $< U >$ varies with excess volume density $\Delta\rho_V$ for the case of $\mu = 0$. The line of black circle is obtained from DEM simulations of non-affine compression. The line of blue star is obtained from numerical simulations of affine compression. The blue dotted line shows the theoretical function for affine compression without new contacts. The black solid line is a fitting curve for DEM data

these functions can be given by the data of numerical simulations. We see from the formula (21) that the reduced average overlap $< U >$ is a key parameter for the mechanical response of packings under deformation. In Fig. 4, we show the variation of $< U >$ with $\Delta\rho_V$ for both the affine compression and the non-affine compression for frictionless packings. The DEM results of average reduced overlap can be fitted very well by a linear function $< U >= K_U\Delta\rho_V$ where $K_U \approx 0.345$. Using Eq. (26), we can derive $< U >= 1-(\rho_V/(\rho_{VC}+\Delta\rho_V))^{1/2}$. This is the theoretical result for packings under affine compression starting from the jamming point without generating new contacts and it is plotted in Fig. 4. We also illustrate the numerical result for affine compression with generating new contacts by data points which are called affine compression in this figure. These results indicate that a packing of frictionless disks will undergo a non-affine deformation even in the case of isotropic compression. The non-affine compression causes a lower response for

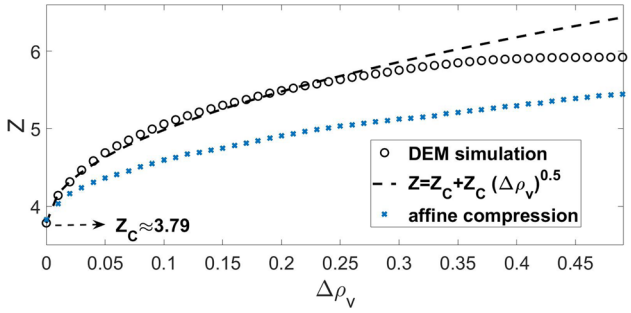

Fig. 5 Average contact number Z varies with excess volume density $\Delta\rho_V$ for the case of $\mu = 0$. Z is counted with ratters and Z_C indicates the critical point of jamming transition. The line of black circle is obtained from DEM simulations of non-affine compression. The line of blue star is obtained from numerical simulations of affine compression. The black dashed line is a fitting curve for DEM data where the fitting formula is the well-known square root relation for Z varying with $\Delta\rho_V$ near the jamming point [24]

$< U >$ than the prediction of affine compression. This result can be understood by applying an infinitesimal affine compression on the packing first and then relaxing the disks to obtain the static state. The process of relaxation incline to the local minimal energy state, therefore a smaller value of $< U >$ is obtained for the non-affine compression.

The change of contact number in loading test is also important to the bulk properties of jammed matter [3,22,28]. In many simulation works, the average contact number is counted with removing all rattlers. Here, we calculate the average contact number Z by using the formula (7) in which rattlers are included, because this definition is more convenient for relating Z to other quantities. As shown in Fig. 5, the critical value of average contact number for frictionless packings is $Z_C \approx 3.79$; Z increases sharply near the jamming point with increasing $\Delta\rho_V$ and then approaches a saturation value $Z_S = 6$. The function $Z = Z_C + Z_C\sqrt{\Delta\rho_V}$ is used to present the scaling law of frictionless spheres near the jamming point [3,24]. We find that the DEM data of $Z(\Delta\rho_V)$ can be fitted well by this function when $\Delta\rho_V < 0.26$, however the difference between them is apparent when $\Delta\rho_V > 0.26$. The numerical results of affine compression starting from jamming point are also illustrated in Fig. 5. Evidently, more contacts are generated for the non-affine compression than the affine compression at the same value of excess volume density. DEM results shown in Fig. 6 tell us that $< U^2 >$ can be replaced by $< U >^2$ in formula (21) as a good approximation.

Next, we investigate the reduced pressure $P^*(\Delta\rho_V)$ and the reduced bulk modulus $K^*(\Delta\rho_V)$. Considering the formula (21) and the numerical results in Figs. 4 and 6, $P^*(\Delta\rho_V)$ can be written as

$$P^* \approx \frac{1}{4\pi}\frac{\langle D^2\rangle}{\langle r^2\rangle}K_U(1-K_U\Delta\rho_V)(\rho_{VC}+\Delta\rho_V)Z\Delta\rho_V$$

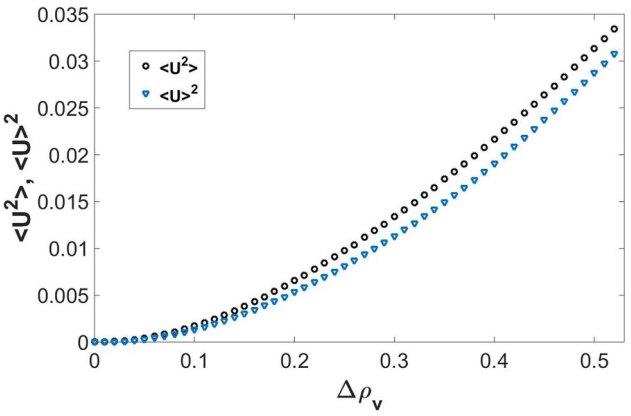

Fig. 6 Average of square reduced overlap $< U^2 >$ and square of average reduced overlap $< U >^2$ vary with excess volume density $\Delta\rho_V$ for the case of $\mu = 0$

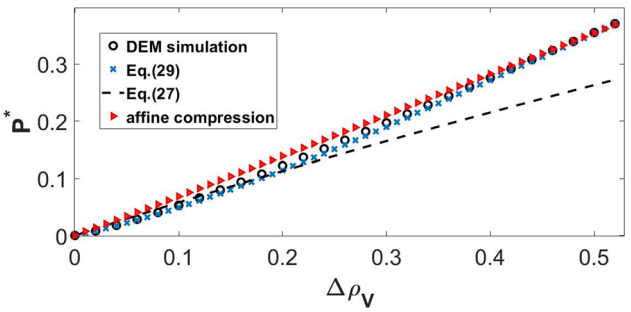

Fig. 7 Reduced pressure P^* varies with excess volume density $\Delta\rho_V$ for the case of $\mu = 0$. The line of black circle is obtained from DEM simulations of non-affine compression. The line of red triangle is obtained from numerical simulations of affine compression. The line of blue cross represents the theoretical results combining with the DEM results of $< U >$ and Z. The black dashed line represents the theoretical function for affine compression without new contacts

(29)

where $\frac{\langle D^2 \rangle}{\langle r^2 \rangle} \approx 3.95$ is calculated by using the formula (20) in which we set $k_B = k_S = 0.5, \lambda = 1.4$. In Fig. 7, the DEM simulation curve of P^* is calculated by using the definition of P_a. In this figure, the numerical results of Eq. (29) are calculated by substituting the DEM data of Z in this equation. We know that Eq. (29) is derived based on the definition of P_b. As shown in Fig. 7, Eq. (29) gives precise prediction for the behavior of $P^*(\Delta\rho_V)$ and this can be seen as a proof that P_a and P_b are statistically equivalent. In this figure, the curve of Eq. (27) is the pressure for the affine compression without new contacts. Apparently, the difference of the pressure curves between non-affine compression and affine compression without new contacts is large for large $\Delta\rho_V$. However, the difference of the pressure curves between non-affine compression and affine compression is very small for the whole range of $\Delta\rho_V$.

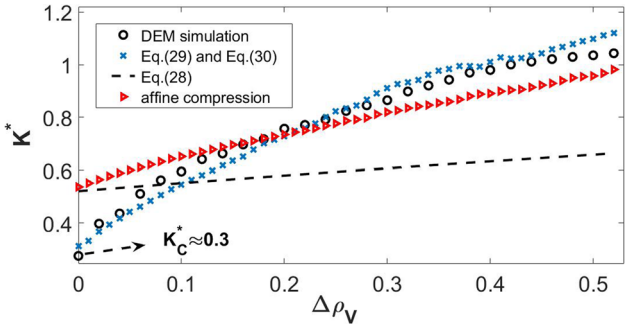

Fig. 8 Reduced bulk modulus K^* varies with excess volume density$\Delta\rho_V$ for the case of $\mu = 0$. K_C^* indicates the reduced bulk modulus at jamming point. The line of black circle is obtained from DEM simulations of non-affine compression. The line of red triangle is obtained from numerical simulations of affine compression. The line of blue cross represents the theoretical results combining with the DEM results of $< U >$ and Z. The black dashed line represents the theoretical function for affine compression without new contacts

Considering the formula (28), the reduced bulk modulus can be calculated by

$$K^* = (\rho_{VC} + \Delta\rho_V)\frac{\mathrm{d}P^*}{\mathrm{d}\Delta\rho_V} \tag{30}$$

In Fig. 8, the DEM simulation curve of K^* is calculated by obtaining $P^*(\Delta\rho_V)$ through the definition of P_a first and then computing the formula (30). It corresponds to the non-affine compression. We find that the reduced bulk modulus increases sharply starting from a nonzero value $K_C^* \approx 0.3$ with increasing $\Delta\rho_V$. The curve obtaining from Eqs. (29) and (30) is quite close to the DEM simulation curve of K^*. This indicates that the formula (30) is suitable not only for the discussion of pressure but also for the discussion of reduced bulk modulus. Seeing the curve of Eq. (28), the range of K^* of affine compression without new contacts is much smaller than the one of non-affine compression. The main reason for this is that the generating of new contacts is ignored and $Z(\rho_V)$ is set as a constant Z_C. Even when the generating of new contacts is considered, the difference of $K^*(\Delta\rho_V)$ between non-affine compression and affine compression is apparent. Evidently, the value of K^* of non-affine is much smaller than the one of affine compression for the case of $\Delta\rho_V \to 0$. The main reason is that the change rate of $\bar{U}(\Delta\rho_V)$ of non-affine compression is smaller than the one of affine compression when $\Delta\rho_V \to 0$ (see Fig. 4).

4.2 Bulk properties of frictional disks

Static friction plays an important role in the structural and mechanical properties of particulate systems [3,13,14,29]. To understand how the bulk properties of amorphous packings are affected by static friction, we also perform the DEM simulations on frictional pack-

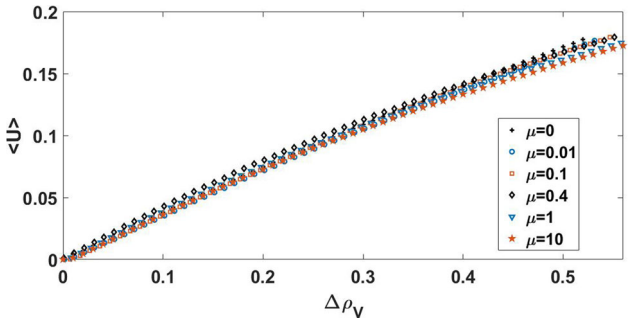

Fig. 9 Average reduced overlap $< U >$ varies with excess volume density $\Delta\rho_V$ for different friction coefficients μ

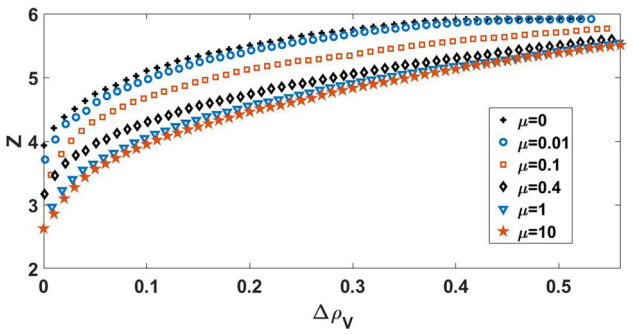

Fig. 10 Average contact number Z varies with excess volume density $\Delta\rho_V$ for different friction coefficients μ

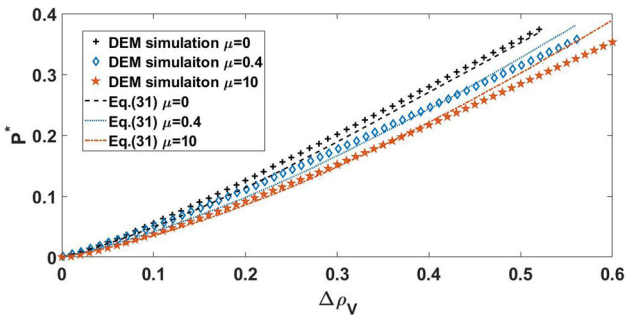

Fig. 11 Reduced pressure P^* varies with excess volume density $\Delta\rho_V$ for different friction coefficients μ

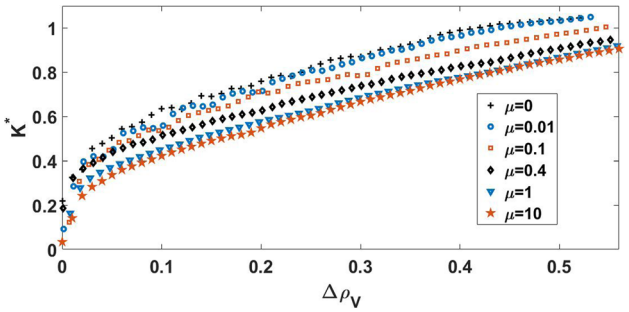

Fig. 12 Reduced bulk modulus K^* varies with excess volume density $\Delta\rho_V$ for different friction coefficients μ

ings of bidisperse disks under isotropic compression. As shown in Fig. 2, the slope of the curve $P^*(\Delta\rho_V)$ is changed by the variation of μ. To understand this deeply, we show the DEM results of $\bar{U}(\Delta\rho_V)$ and $Z(\Delta\rho_V)$ with different values of μ in Figs. 9 and 10 respectively. Evidently, $\bar{U}(\Delta\rho_V, \mu)$ changes by a very small mount while $Z(\Delta\rho_V, \mu)$ presents obvious decrease with the increasing μ at a fixed $\Delta\rho_V$. According to Eq. (21), the decrease of $Z(\Delta\rho_V, \mu)$ will cause the decrease of $P^*(\Delta\rho_V, \mu)$ with a fixed $\Delta\rho_V$. As shown in Fig. 11, this prediction agrees with the DEM results of $P^*(\Delta\rho_V, \mu)$.

Since $\bar{U}(\Delta\rho_V, 0) \approx K_U\Delta\rho_V$ where $K_U \approx 0.345$, we could take$\bar{U}(\Delta\rho_V, \mu) \approx K_U\Delta\rho_V$ as a good approximation for all values of μ according to Fig. 9. Therefore, the reduced pressure $P^*(\Delta\rho_V, \mu)$ could be calculated theoretically by using Eq. (29) if $\rho_{VC}(\mu)$ and $Z(\Delta\rho_V, \mu)$ are given. Figure 2 shows that $\rho_{VC}(\mu)$ decreases by a very small mount with the increasing μ from 0 to 10. Hence, we could take $\rho_{VC}(\mu) \approx \rho_{VC}(0) = 0.831$ in Eq. (29). As mentioned previously, $\dfrac{\langle D^2\rangle}{\langle r^2\rangle} \approx 3.95$ is the result of Eq. (20) for the case of $k_B = k_S = 0.5, \lambda = 1.4$. Substitute these values into Eq. (29), we have

$$P^*(\Delta\rho_V, \mu) \approx 0.108(1-0.345\Delta\rho_V)(0.831+\Delta\rho_V)\Delta\rho_V Z(\Delta\rho_V, \mu) \quad (31)$$

where the value of $Z(\Delta\rho_V, \mu)$ could be given according to the DEM results in Fig. 10. In Fig. 11, DEM simulation results are compared with the theoretical results obtaining from Eq. (31). This figure shows that most of the simulation data are very close to the prediction from Eq. (31) except for the data for large $\Delta\rho_V$ and large μ. The large deviation in the case of large $\Delta\rho_V$ and large μ may be caused by the assumption of $\bar{U}(\Delta\rho_V, \mu) \approx K_U\Delta\rho_V$. We could also see from Fig. 11 that the slope of $P^*(\Delta\rho_V)$ decreases with the increasing μ and this must cause the decrease of reduced bulk modulus of soft disks. As shown in Fig. 12, $K^*(\Delta\rho_V, \mu)$ does decrease with the increasing μ at a fixed $\Delta\rho_V$ and we could sum up the main reason as the decrease of average contact number.

5 Conclusions

In this article, we combine the DEM simulations and theoretical analysis to study the bulk properties of soft disks under isotropic compression. In the part of theoretical research, through microscopic and statistical analysis, we derive some relations between different macroscopic quantities, such as Eqs. (13) and (15). Then, these relations are used to investigate packings with linear interactions and systems under affine compression, and the theoretical formulae of reduced pressure and reduced bulk modulus are derived for systems under affine compression without new contacts. In the

part of numerical simulation, we perform the DEM simulations on disordered packings of frictionless and frictional disks with linear interactions and then compare the DEM results with the results of theoretical analysis. We find several important results on how P^* and K^* are affected by the non-affine compression and the variation of μ. (1) The behaviors of the average contact number $Z(\Delta\rho_V, \mu)$ and the average reduced overlap $\bar{U}(\Delta\rho_V, \mu)$ are the key to understand the mechanical properties of jammed matter. Affine deformation and non-affine deformation cause different behaviors on $Z(\Delta\rho_V)$ and $\bar{U}(\Delta\rho_V)$ and therefore the effect of non-affine deformation should be taken into account to correctly derive the behaviors of mechanical properties especially the one of $K^*(\Delta\rho_V)$. (2) An interesting result is that $\bar{U}(\Delta\rho_V, \mu)$ varies approximately linear with $\Delta\rho_V$ over a wide range and it is hardly changed with the variation of μ. This means that the non-affine deformation cause a simple behavior for $\bar{U}(\Delta\rho_V, \mu)$. However, the non-affine deformation causes a complex behavior for $Z(\Delta\rho_V, \mu)$. The variation of $Z(\Delta\rho_V, \mu)$ is the key to understand why the slope of $P^*(\Delta\rho_V)$ and the value of $K^*(\mu)$ decrease with increasing μ. It should be noticed that we only consider the linear contact model and the variation range of $\Delta\rho_V$ is huge in this paper. For an actual particulate system, the linear contact force law is not likely tenable over such huge deformation between two contacted particles. Despite all this, the microscopic contact force law is only one of the factors that influence the behaviors of mechanical properties of jammed matter. Therefore, our research is still meaningful to clarify the behaviors of jammed matter under isotropic compression.

Acknowledgements We acknowledge support from the China Scholarship Council (Grant No. 201806675016) and the National Natural Science Foundation of China (Grant No. 11965007). We also thank Mark D. Shattuck for useful discussions and the visiting program provided by Hernán A. Makse.

Declarations

Conflict of interest The authors declare that they have no known competing financial interests or personal relationships that could have appeared to influence the work reported in this paper.

References

1. A.J. Liu, S.R. Nagel, Jamming is not just cool any more[J]. Nature **396**(5), 21–22 (1998). https://doi.org/10.1038/23819
2. S. Torquato, F..H. Stillinger, Jammed hard-particle packings: from Kepler to Bernal and beyond[J]. Rev. Mod. Phys. **82**(3), 2633–2672 (2010). https://doi.org/10.1103/RevModPhys.82.2633
3. M. van Hecke, Jamming of soft particles: geometry, mechanics, scaling and isostaticity[J]. J. Phys.: Condens. Matter **22**(3), 033101 (2010). https://doi.org/10.1088/0953-8984/22/3/033101
4. A. Baule, F. Morone, H.J. Herrmann, H.A. Makse, Edwards statistical mechanics for jammed granular matter[J]. Rev. Mod. Phys. **90**(1), 015006:1-015006:58 (2018). https://doi.org/10.1103/revmodphys.90.015006
5. C.S. O'Hern, S.A. Langer, A.J. Liu, S.R. Nagel, Random packings of frictionless particles[J]. Phys. Rev. Lett. **88**(7), 075507 (2002). https://doi.org/10.1103/PhysRevLett.88.075507
6. T.S. Majmudar, M. Sperl, S. Luding, R.P. Behringer, Jamming transition in granular systems[J]. Phys. Rev. Lett. **98**(5), 058001 (2007). https://doi.org/10.1103/PhysRevLett.98.058001
7. P. Chaudhuri, L. Berthier, S. Sastry, Jamming transitions in amorphous packings of frictionless spheres occur over a continuous range of volume fractions[J]. Phys. Rev. Lett. **104**, 1345–1358 (2010). https://doi.org/10.1103/PhysRevLett.104.165701
8. C. Zhao, K. Tian, N. Xu, New jamming scenario: from marginal jamming to deep jamming[J]. Phys. Rev. Lett. **106**(12), 125503 (2011). https://doi.org/10.1103/PhysRevLett.106.125503
9. K. Saitoh, V. Magnanimo, S. Luding, A Master equation for the probability distribution functions of forces in soft particle packings[J]. Soft matter **11**(7), 1253–1258 (2015) https://pubs.rsc.org/en/content/articlelanding/2015/SM/C4SM02452D#!divAbstract
10. H. Mizuno, K. Saitoh, L.E. Silbert, Elastic moduli and vibrational modes in jammed particulate packings[J]. Phys. Rev. E **93**(6), 062905 (2016). https://doi.org/10.1103/PhysRevE.93.062905
11. T. Bertrand, R.P. Behringer, B. Chakraborty, C.S. O'Hern, M.D. Shattuck, Protocol dependence of the jamming transition[J]. Phys. Rev. E **93**(1), 012901 (2016). https://doi.org/10.1103/PhysRevE.93.012901
12. S. Chen, T. Bertrand, W.W. Jin, M.D. Shattuck, C.S. O'Hern, Stress anisotropy in shear-jammed packings of frictionless disks[J]. Phys. Rev. E **98**, 042906 (2018). https://doi.org/10.1103/PhysRevE.98.042906
13. D.P. Bi, J. Zhang, B. Chakraborty, R.P. Behringer, Jamming by shear[J]. Nature **480**, 355–358 (2011). https://doi.org/10.1038/nature10667
14. S. Papanikolaou, C.S. O'Hern, M.D. Shattuck, Isostaticity at frictional jamming[J]. Phys. Rev. Lett. **110**(19), 198002 (2013). https://doi.org/10.1103/PhysRevLett.110.198002
15. K. VanderWerf, W.W. Jin, M.D. Shattuck, C.S. O'Hern, Hypostatic jammed packings of frictionless nonspherical particles[J]. Phys. Rev. E **97**(1), 012909 (2018). https://doi.org/10.1103/PhysRevE.97.012909
16. Z.H. Xu, R. Wang, J.M. Cui, Y.J. Liu, W. Zheng, Effects of short-range attraction on Jamming transition[J]. Chin. Phys. B **30**, 066101 (2021). https://doi.org/10.1088/1674-1056/abefc5
17. A. Boromand, A. Signoriello, F.F. Ye, C.S. O'Hern, M.D. Shattuck, Jamming of deformable polygons[J]. Phys. Rev. Lett. **121**(24), 248003 (2018). https://doi.org/10.1103/PhysRevLett.121.248003
18. A.N. Norris, D.L. Johnson, Nonlinear elasticity of granular media[J]. J. Appl. Mech. Mar **64**, 39–49 (1997). https://doi.org/10.1115/1.2787292

19. S. Alexander, Amorphous solids: their structure, lattice dynamics and elasticity[J]. Phys. Rep. **296**, 65–236 (1998). https://doi.org/10.1016/S0370-1573(97)00069-0
20. H.A. Makse, D.L. Johnson, L.M. Schwartz, Packing of compressible granular materials[J]. Phys. Rev. Lett. **84**(18), 4160–4163 (2000). https://doi.org/10.1103/PhysRevLett.84.4160
21. H.A. Makse, N. Gland, D.L. Johnson, L. Schwartz, Granular packings: nonlinear elasticity, sound propagation, and collective relaxation dynamics[J]. Phys. Rev. E **70**, 061302-1-061302–19 (2004). https://doi.org/10.1103/PhysRevE.70.061302
22. W.G. Ellenbroek, Non-affine response: Jammed packings vs. spring networks[J]. Europhys. Lett. **87**(3), 34004 (2009). https://doi.org/10.1209/0295-5075/87/34004
23. B.Y. Cui, G. Ruocco, A. Zaccone, Theory of elastic constants of athermal amorphous solids with internal stresses[J]. Granular Matter **21**(3), 69 (2019). https://doi.org/10.1007/s10035-019-0916-4
24. W. Zheng, S.Y. Zhang, N. Xu, Jamming of packings of frictionless particles with and without shear[J]. Chin. Phys. B **27**, 066102 (2018). https://doi.org/10.1007/s10035-019-0916-4
25. M.P. Ciamarra, P. Sollich, The first jamming crossover: geometric and mechanical features[J]. J. Chem. Phys. **138**(12), 12A529 (2013). https://doi.org/10.1063/1.4779181
26. P.A. Cundall, O.D.L. Strack, A discrete numerical model for granular assemblies[J]. Geotechnique **29**, 47–65 (1979) http://websrv.cs.umt.edu/classes/cs477/images/0/0e/Cundall_Strack.pdf
27. W. Zhang, L. Hu, X.G. Zhang, Structural features of critical jammed state in bi-disperse granular systems. Acta Physica Sinica **65**(2), 024502 (2016). https://doi.org/10.7498/aps.65.024502
28. N. Kumar, V. Magnanimo, M. Ramaioli, S. Luding, Tuning the bulk properties of bidisperse granular mixtures by small amount of fines[J]. Powder Technol. **293**, 94–112 (2016)
29. H.A. Vinutha, S. Sastry, Disentangling the role of structure and friction in shear jamming[J]. Nature Phys. **12**(6), 578–583 (2016). https://doi.org/10.1038/nphys3658